JOURNAL OF TISSUE ENGINEERING AND REGENERATIVE MEDICINE
J Tissue Eng Regen Med (2012)
Published online in Wiley Online Library (wileyonlinelibrary.com) **DOI:** 10.1002/term.1575

RESEARCH ARTICLE

Time-lapse microscopy and classification of 2D human mesenchymal stem cells based on cell shape picks up myogenic from osteogenic and adipogenic differentiation

Christof Seiler[1], Amiq Gazdhar[2], Mauricio Reyes[1], Lorin M. Benneker[3], Thomas Geiser[2], Klaus A. Siebenrock[3] and Benjamin Gantenbein-Ritter[1,4]*
[1]*Institute for Surgical Technology and Biomechanics, University of Bern, Switzerland*
[2]*Department of Pulmonary Medicine, Insel University Hospital, Bern, Switzerland*
[3]*Orthopaedic Department, Insel University Hospital, Bern, Switzerland*
[4]*ARTORG Centre for Biomedical Engineering Research, University of Bern, Switzerland*

Abstract

Current methods to characterize mesenchymal stem cells (MSCs) are limited to CD marker expression, plastic adherence and their ability to differentiate into adipogenic, osteogenic and chondrogenic precursors. It seems evident that stem cells undergoing differentiation should differ in many aspects, such as morphology and possibly also behaviour; however, such a correlation has not yet been exploited for fate prediction of MSCs. Primary human MSCs from bone marrow were expanded and pelleted to form high-density cultures and were then randomly divided into four groups to differentiate into adipogenic, osteogenic chondrogenic and myogenic progenitor cells. The cells were expanded as heterogeneous and tracked with time-lapse microscopy to record cell shape, using phase-contrast microscopy. The cells were segmented using a custom-made image-processing pipeline. Seven morphological features were extracted for each of the segmented cells. Statistical analysis was performed on the seven-dimensional feature vectors, using a tree-like classification method. Differentiation of cells was monitored with key marker genes and histology. Cells in differentiation media were expressing the key genes for each of the three pathways after 21 days, i.e. adipogenic, osteogenic and chondrogenic, which was also confirmed by histological staining. Time-lapse microscopy data were obtained and contained new evidence that two cell shape features, eccentricity and filopodia (= 'fingers') are highly informative to classify myogenic differentiation from all others. However, no robust classifiers could be identified for the other cell differentiation paths. The results suggest that non-invasive automated time-lapse microscopy could potentially be used to predict the stem cell fate of hMSCs for clinical application, based on morphology for earlier time-points. The classification is challenged by cell density, proliferation and possible unknown donor-specific factors, which affect the performance of morphology-based approaches.
Copyright © 2012 John Wiley & Sons, Ltd.

Received 26 February 2012; Revised 21 May 2012; Accepted 15 June 2012

Keywords **time-lapse microscopy; mesenchymal stem cells; real-time RT–PCR; histology; segmentation; cell shape; filopodia**

1. Introduction

Autologous human mesenchymal stem cells (hMSCs) have been proposed as a major source for regenerative therapy for the musculoskeletal system (Giordano *et al.*, 2007;

**Correspondence to: B. Gantenbein-Ritter, University of Bern, Medical Faculty, ARTORG Centre for Biomedical Engineering Research, Institute for Surgical Technology and Biomechanics, Stauffacherstrasse 78, CH-3014 Bern, Switzerland. E-mail: Benjamin.Gantenbein@istb.unibe.ch*

Copyright © 2012 John Wiley & Sons, Ltd.

Caplan, 1991; Pittenger, 2008; Chamberlain, 2006; Prockop, 1997, 2001). The reason for this is three-fold: first, these cells can be isolated from the human body (bone-marrow, adipose tissue); second, these cells can be expanded rapidly in vitro (Caplan, 1991, 2005; Pittenger *et al.*, 1999); third, there is no ethical controversy regarding their use. The natural stem-cell 'niche' of these cells, however, has not been described in detail and current laboratory practice is to expand the cells as a mixed and heterogeneous cell population, starting from a few founder cells (Chamberlain, 2006; da Silva Meirelles *et al.*, 2008). The International Society for Cellular Therapy defined the minimal standards for a stromal cell population to be called 'hMSCs': first, the MSCs must be plastic-adherent when maintained in standard culture conditions; second, the MSCs must express CD105, CD73 and CD90 and lack expression of CD45, CD34, CD14 or CD11b, CD79a or CD19 and HLA-DR surface molecules; third, the MSCs must differentiate to osteoblasts, adipocytes and chondroblasts in vitro (Dominici *et al.*, 2006). However, this definition still does not define the source pool of these cell populations, neither does it tell about the heterogeneity of these cells and also its outcome.

hMSCs have attracted immense research interest in the field of regenerative medicine, due to their ability to be cultured for successive passages and multi-lineage differentiation. However, the molecular mechanisms governing MSCs self-renewal and differentiation remain largely unknown. The self-renewal capability of MSCs was only recently proven with 'true single cell clonal tracing' of lineages (Sarugaser *et al.*, 2009). However, the heterogenic nature of these stem cell populations has been noted to be a major source of variance (Sengers *et al.*, 2009; Solchaga *et al.*, 1999; Roeder and Radtke, 2009). The development of sophisticated techniques, in particular clinical proteomics, has enabled researchers in various fields to identify and characterize cell-specific biomarkers for therapeutic purposes. For instance, a recent study tried to understand the cellular and subcellular processes responsible for the existence of stem cell populations in bone marrow samples, by revealing the whole cell proteome of the clonal cultures of bone marrow-derived MSCs (Mareddy *et al.*, 2009). However, all of these methods require invasive manipulation of these cells and the use of some sort of labelling or real-time reverse transcription (RT)–PCR technique to confirm the phenotype of these cells for downstream analyses or direct clinical application. Clinical application to inject these expanded cells into any tissue, such as the intervertebral disc, would require prior knowledge about the differentiation state of these cells (Dainiak *et al.*, 2007). Here, we propose the characterization of hMSCs without direct invasive manipulation of these cells, using an approach herewith termed 'statistical stem cell' modelling, involving microscopic imaging and advanced image-processing algorithms. The primary aim of this study was to observe the shape of primary hMSCs cells undergoing differentiation on standard culture plastic under in vitro controlled conditions and to evaluate any correlations between the shapes of stem cells, cell type and differentiation pathways. Hence, here we evaluate any correlations between the shapes of stem cells and their fates during the differentiation process of primary human MSCs in two-dimensional (2D) cell culture.

2. Materials and methods

2.1. Cell source and expansion

Human bone marrow was harvested from a patient undergoing spine surgery, with written consent. The procedure was approved by the local Ethics Office (KEK No. 187/10). hMSCs were amplified from 'buffy coat' after density gradient centrifugation by selection for plastic adherence. Passage 3 cells were seeded onto standard plastic culture plates (Falcon, VWR, Switzerland) in inductive media for osteogenic, adipogenic, myogenic, three-dimensional (3D) alginate chondrogenic (not live-tracked) and control and kept in culture for 21 days. Time-lapse imaging was conducted using IncuCyte Plus® (Essen BioScience, Bucher, Switzerland) for 6 days. At the end of the experiments, cell phenotype during differentiation was monitored by real-time RT–PCR analysis of key genes, such as transcription factors, which are characteristic for the osteogenic, adipogenic, myogenic and chondrogenic pathways (Table 1).

2.2. CD marker characterization

Cells were trypsinized and resuspended in phosphate-buffered saline (PBS) containing 0.5% bovine serum albumin (BSA) and were stained with antibodies as given in Table 1. 2 μl antibody reaction solution, as provided from the manufacturer (Becton–Dickinson, Allschwil, Switzerland) was added to 2.5×10^5 cells and incubated for 30 min with the cells. The antibodies were then removed and the cells were washed with PBS containing 0.5% BSA and kept therein until measured. The cells were characterized on a BD™ LSR II (BD Pharmagen, Brussels, Belgium), using forward- and side-scatter and lasers for the specific dyes FITC, PE, AlexaFluor 488, PE-Cy5 and PE-Cy7 (Table 2).

Table 1. Table of analysed parameters to identify multipotentiality of isolated plastic-adherent hMSCs

Pathway	Gene expression	Histology
Osteogenesis	*col1*, *OPN*	von Kossa, fast red
Adipogenesis	*Adiponectin*	Oil red O/Meyer's haematoxylin
Chondrogenesis	*ACAN*, *col2*	Safranin O/fast green/alcian blue
Myogenesis	*MyoD*, *Desmin*	α-sm actin, MyoD

Copyright © 2012 John Wiley & Sons, Ltd.

DOI: 10.1002/term

2.3. Stem cell differentiation

Primary hMSCs cells were passaged and $\sim 10^4$ cells were seeded into six-well plates and allowed to grow and differentiate for up to 21 days. For chondrogenic differentiation, the cells were seeded in 1.2% alginate (Fluka, Sigma-Aldrich, Buchs, Switzerland) with 4 million cells/ml (Mehlhorn *et al*., 2006; Gantenbein-Ritter *et al*., 2011). Beads were produced by steadily pressing the cell suspension through a syringe equipped with a 22G needle into 102 mM $CaCl_2$ 0.9% NaCl solution, as previously described (Gantenbein-Ritter *et al*., 2011).

The stem cells were differentiated in the following media (treatments):

- *Adipogenic induction medium* (AIM), consisting of α-modified Eagle's medium (αMEM) containing 10% fetal bovine serum (FBS), antibiotics, 0.5 mM methyl isobutylxanthine, 1 μM dexamethasone, 10 μg/ml insulin and 100 μM indomethacin.
- *Chondrogenic differentiation medium* (CHDM), consisting of high-glucose (4.5 g/l) Dulbecco's modified Eagle's medium (DMEM) supplemented with 6.25 μg/ml insulin, 6.25 μg/ml transferrin, 6.25 μg/ml selenous acid, 5.33 μg/ml γ-linoleic acid and 1.25 mg/ml BSA (ITS^+, Sigma-Aldrich), 0.1 μM dexamethasone, 10 ng/ml transforming growth factor-β1 (TGFβ1; Peprotech, London, UK), 50 μg/ml ascorbate 2-phosphate, 2 mM pyruvate and antibiotics.
- HMSCs were seeded in 1.2% alginate (Fluka, Sigma-Aldrich) at a density of 4×10^6 cells/ml.
- *Osteogenic supplemented medium* (OSM), consisting of DMEM with 10% fetal calf serum (FCS) with osteogenic supplements 50 μM ascorbate 2-phosphate, 10 mM glycerol phosphate and 100 nM dexamethasone.
- *Myogenic medium* (MYM): induced cells were placed in myogenic supplemented (MS) medium comprising 88% α-MEM, 10% antibiotics, 10% FBS, 1 nM dexamethasone (Sigma-Aldrich) and 2 μM hydrocortisone (Sigma-Aldrich). The culture medium was replaced every 3 days until multinucleated myotubes could be observed (28 days).

2.4. Time-lapse microscopy settings

The cells of the heterogeneous hMSCs population were monitored using an Incucyte Plus® time-lapse microscope, which was put into a standard incubator at 5% CO_2, 95% humidity. The software of the microscope was configured to take an image of each well every 2 h from the start of the differentiation experiment, i.e. the imaging started ~20 min after seeding the cells and was then continued for 6 days, with a 20 min break for media refreshment after 3 days. This covered the exponential growing phase until confluence. The data were collected as Tiff images and processed using a customized image pipeline, as described below.

2.5. Analysis of time-lapse microscopy data and segmentation algorithms

Differentiation of cells was monitored with key marker genes and histology. Cells were segmented using a custom-made image processing pipeline. The segmentation pipeline was implemented in order to distinguish cells from the background. The segmentation pipeline is composed of standard image-processing operations in the following order: 1, original image (Figure 1.1); 2, Sobel edge detection (Figure 1.2); 3, image dilation (Figure 1.3); 4, removal of objects close to image borders (Figure 1.4); 5, image erosion (Figure 1.5); 6, removal of small objects (Figure 1.6); 7, filling of gaps inside the cell (Figure 1.7); and 8, overlay of the final result on the original image (Figure 1.8). Seven morphological features were extracted from each of the segmented cells. The feature space in which we performed statistical classification was therefore seven-dimensional (7D; one vector for each cell), with the following features: area, major and minor axis lengths, perimeter, eccentricity, extent, and number of fingers. Statistical analysis was performed on the 7D feature vectors, using a tree-like classification method called the 'node harvest' method, which was introduced by Meinshausen (2010). The developed Matlab™ and R routines are available at: http://www.mathworks.ch/matlabcentral/fileexchange/ on the webpage of Mathworks Inc. under the project name 'cell shape classifier'.

2.6. Feature vector

Once the cells were segmented, we extracted the following 7D feature vectors (Figure 2):

1. *Area*: the number of pixels to a cell.
2. *Major axis length*: scalar specifying the length (in pixels) of the major axis of a cell.
3. *Minor axis length*: the length (in pixels) of the minor axis of a cell
4. *Perimeter*: the distance around the boundary of a cell.
5. *Eccentricity*: scalar that specifies the eccentricity of the cell. The eccentricity is the ratio of the distance between the foci of the cell and its major axis length. The value ranges from 0 to 1, where 0 represents circular cells and 1 cells that are stretched out to a line.
6. *Extent*: scalar that specifies the ratio of pixels inside the cell to pixels in the enclosing box.
7. *Finger*: thresholded result of the Poisson equation with boundary condition set to 0 at the contour of the cell.

In Gorelick *et al*. (2006), the authors used the same algorithm to identify human fingers. Here, we took advantage of the analogy between human fingers and cell 'fingers'.

2.7. Statistical Analysis using the node harvest method

We applied the node harvest method (Meinshausen, 2010) to classify feature vectors. Node harvest is a statistical

Copyright © 2012 John Wiley & Sons, Ltd.

DOI: 10.1002/term

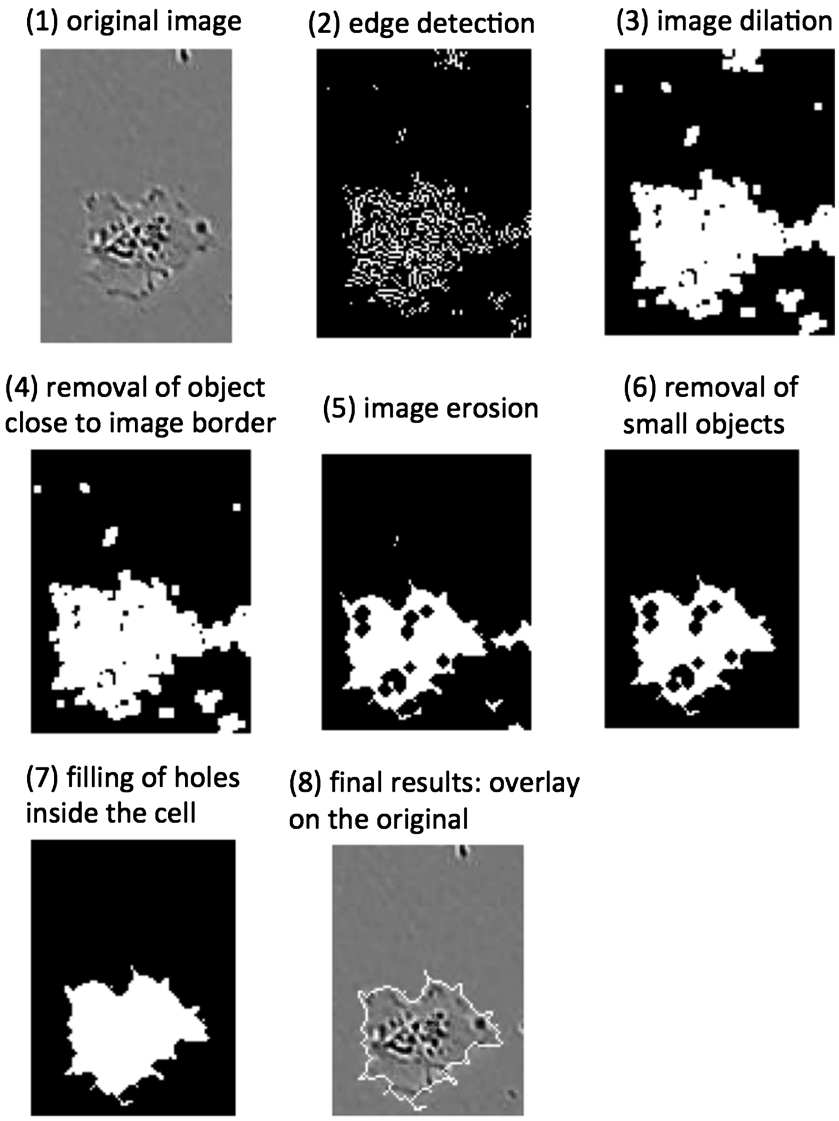

Figure 1. (A–H) Illustration of the segmentation pipeline that was used to extract cells from phase-contrast images (×10 magnification). The time-lapse microscope (Incucyte, Essen Bioscience) series was used

classification technique that combines interpretability and prediction accuracy and is especially suited for low signal:noise ratio data, due to its robust estimation process.

Node harvest starts by randomly generating a few thousands nodes. Each node represents a set of observations, in our case the cells, and a set of conditions, in our case elements of the feature vector. For instance, in Figure 6B, the node at the bottom right contains 720 cells (y axis) with the property $0.96 \leq$ eccentricity. The size of the node indicates the importance, which is found through a new type of optimization algorithm favouring sparse solutions. The sparseness reduces the number of nodes in the final plot and enables better interpretability. The connection between nodes represents subsets. Finally, on the x axis the likelihood of one cell belonging to one cell type is shown; as can be seen, there is no discrete classification but a continuous classification, indicating the likelihood of assignment to either one of the cell types.

The only parameter to define is the number of nodes that are randomly generated at the beginning. We obtained stable results by using 1000 nodes. Further, it is possible to constrain the maximum number of conditions/node; we chose one condition/node to maximize interpretability (Meinshausen, 2010).

2.8. Real time RT–PCR

The differentiation process was monitored using 'key genes' for mesenchymal differentiation, i.e. adipogenic, osteogenic, chondrogenic and myogenic. The primers were designed using Beacon designer software (Premier Biosoft, Palo Alto, CA, USA), synthesized at Microsynth (Balgach, Switzerland) and tested for efficiency (around 100%) before using in the experiment (Table 3). Real-time gene expression was monitored and ribosomal *18S* was used as a reference gene (Livak and Schmittgen, 2001; Schmittgen and Zakrajsek, 2000). Around 500 ng total RNA was

Copyright © 2012 John Wiley & Sons, Ltd.

DOI: 10.1002/term

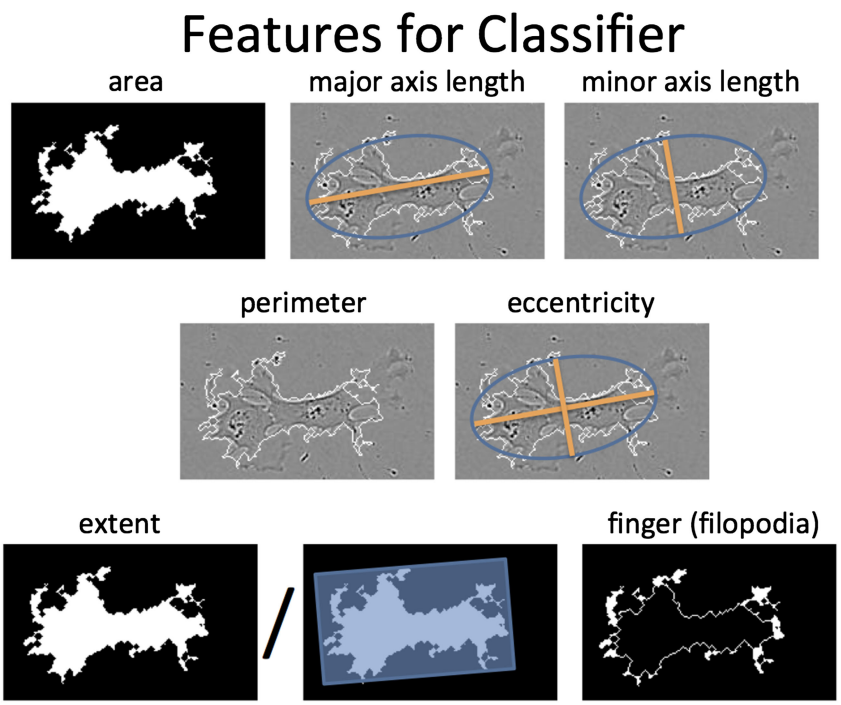

Figure 2. (A–H) The seven shape features that were extracted from each cell for morphological analysis

Table 2. Labelled antibodies for characterization of primary hMSCs

Antigen	Synonym	Supplier	Cat. no.	Fluorophore	Isotype
CD44	Hyaluronan receptor	BD Pharmingen	555478	FITC	Mouse IgG2b, κ
CD90	Thy-1 glycophosphatidylinositol (GPI) anchored conserved cell surface protein	BD Pharmingen	555595	FITC	Mouse IgG1, κ
CD34	Important adhesion molecule for T-lymphocytes	BD Pharmingen	555823	PE-Cy5	Mouse IgG1, κ
CD45	Leukocyte common antigen	BD Pharmingen	557748	PE-Cy7	Mouse IgG1, κ
CD105	Endoglin	Invitrogen	MHCD10520	AlexaFluor 488	Mouse IgG1, κ
CD14	Monocyte differentiation antigen	BD Pharmingen	557742	PE-Cy7	Mouse IgG2a, κ

Table 3. Primers used for real-time RT–PCR

Gene abbreviation	Name	Forward	Reverse
Hs18S	Reference gene	CGA TGC GGC GGC GTT ATT C	TCT GTC AAT CCT GTC CGT GTC C
Chondrogenic differentiation			
ACAN	Aggrecan core protein	CAT CAC TGC AGC TGT CAC	AGC AGC ACT ACC TCC TTC
col1A2	Collagen 1A2	GTG GCA GTG ATG GAA GTG	CAC CAG TAA GGC CGT TTG
col2A1	Collagen 2A1	AGC AAG AGC AAG GAG AAG	GGG AGC CAG ATT GTC ATC
Osteogenic differentiation			
OSC	Osteocalcin	GCA GAG TCC AGC AAA GGTG	CCA GCC ATT GATA CAG GTA GC
OPN	Osteopontin	ACG CCG ACC AAG GAA AAC TC	GTC CATA AAC CAC ACT ATC ACC TCG
Adipogenic differentiation			
APN	Adiponectin	CCG TGA TGG CAG AGA TGG	TATA CATA GGC ACC TTC TCC AG
Myogenic differentiation			
MyoD	Myosin heavy chain	ACA ACG GAC GAC TTC TAT	GTG CTC TTC GGG TTT CAG
DES	Desmin (BD)	GCA GCC AAC AAG AAC AAC	CAA TCT CGC AGG TGT AGG

All primers were run at 61°C annealing temperature (T_a), using a two-step protocol.

reverse-transcribed using the iScript kit (Bio-Rad, Basel, Switzerland). Real-time PCR was then carried out, mixing 5 µl 5× (in 1× Tris–EDTA buffer) diluted cDNA and the IQ SYBR Green Supermix (Bio-Rad) on an IQ5 cycler from Bio-Rad. The two-step amplification profile was 45 cycles of (95°C for 15 s and 61°C for 30 s). All amplicons were analysed using melting curve analysis for the presence of pseudo-genes. Relative gene expression was first calculated relative to the reference gene as ΔC_T values. The relative gene expression was analysed using the $2^{-\Delta\Delta C_T}$ method (Livak and Schmittgen, 2001) and relative to the undifferentiated cells of day 0.

Copyright © 2012 John Wiley & Sons, Ltd.

DOI: 10.1002/term

2.9. Histology

The cells were initially fixed in 4% paraformaldehyde (PFA) directly on the six-well plate and stored at 4°C prior to staining. The cells were rinsed in PBS and then stained with Oil red O and Meyer's haematoxylin or with nuclear fast red and von Kossa silver stain (osteogenic pathway) (Zuk *et al*., 2001). For myogenic differentiation, cells were transferred after 14 days onto glass cover slips in six-well plates, allowed to grow for 72 h and then fixed in 3.7% formalin for immunostaining staining, along with the uninduced negative controls. For immunohistochemistry, fixed cells were first permeabilized with 100% methanol for 2 min and blocked with 10% FBS/PBS for 1 h. The cells were then incubated with mouse-anti-human MyoD primary antibody (Santa Cruz Biotechnology, Santa Cruz, CA, USA) or rabbit anti-human α-smooth muscle actin (α-SMA; A2066, Sigma-Aldrich). After washing, the cells were incubated for 1 h with goat anti-mouse AlexaFluor 555 IgG_1 secondary antibody (Molecular Probes, Invitrogen, Basel, Switzerland) or with goat anti-rabbit FITC (ab6717, Abcam, USA) for α-SMA and then incubated for 1 h in 0.5% BSA PBS and washed thoroughly. Cover slips were mounted in slow-fade gold embedding medium with DAPI (Molecular Probes). The cells were then imaged using a confocal laser scanning microscope (cLSM 510, Carl Zeiss, Jena, Germany).

3. Results

3.1. CD marker characterization

The primary cells at passage 3 were homogeneously positive for CD44, CD105 and CD90 and negative for CD14, CD34 and CD45 (data not shown).

3.2. Stem cell differentiation

Primary hMSCs could be differentiated into osteogenetic, adipogenetic and chondrogenic progenitor cells (Figures 3–5). The cells were differentiating into the four lineages, as detected by relative gene expression of key marker genes (Figure 3), and could also be stained for osteogenic (black calcium deposition) and adipogenic (presence of red oil droplets) activity, starting from day 9 (Figure 4). The adipogenic pathway could be confirmed by the onset of adiponectin (APN) expression (upregulation by a factor of 2000 times; Figure 3). Osteogenic differentiation was found by an increase of osteopontin (*OPN*). The relative gene expression levels of collagen type I and osteocalcin (*OSC*), however, were not considerably different from the levels of the undifferentiated stem cells. Nevertheless, the complete absence of calcium deposits in negative controls (expansion medium and with adipogenic medium, data not shown) could be confirmed using a histological staining for von Kossa calcium deposition. Chondrogenic differentiation could be demonstrated by the significant upregulation of aggrecan (by a factor of 1000) and by the upregulation of collagen type 2 (by a factor of 10^6; Figure 3), as well as an increase in alcian blue staining (Figure 4). Finally, myogenic differentiation was checked by the expression of myosin heavy chain (*MyoD*), which is a transcription factor for myogenesis and of the gene desmin (*DES*), which encodes a muscle-specific class III intermediate filament. MyoD and α-sm actin were also found positively stained by immunohistochemistry, which further confirmed the myogenic differentiation (Figure 5).

3.3. Node harvest

The node harvest algorithm clustered the cells into two branches (Figure 6A–D). Eccentricity (Figure 6A–C) was

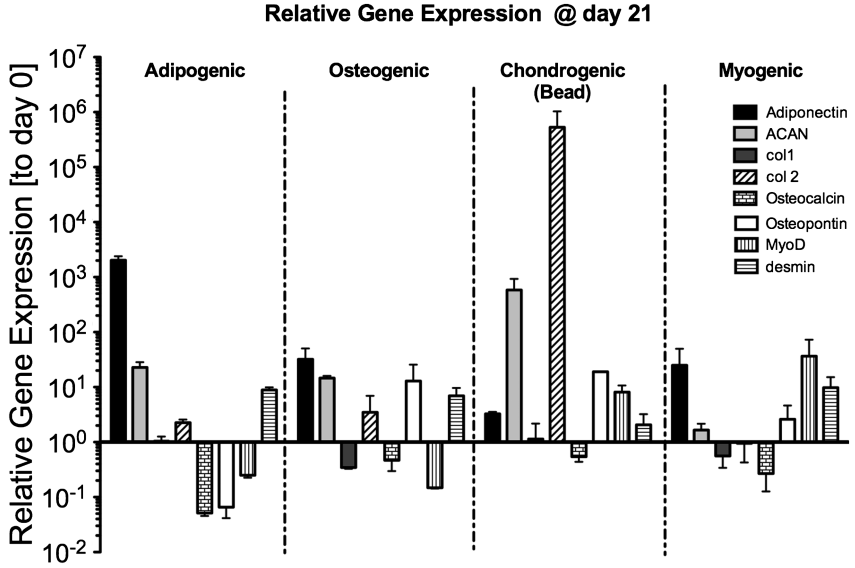

Figure 3. Relative gene expression profiles for marker genes grouped for osteogenic, adipogenic, chondrogenic and myogenic differentiation of hMSCs

Copyright © 2012 John Wiley & Sons, Ltd.

DOI: 10.1002/term

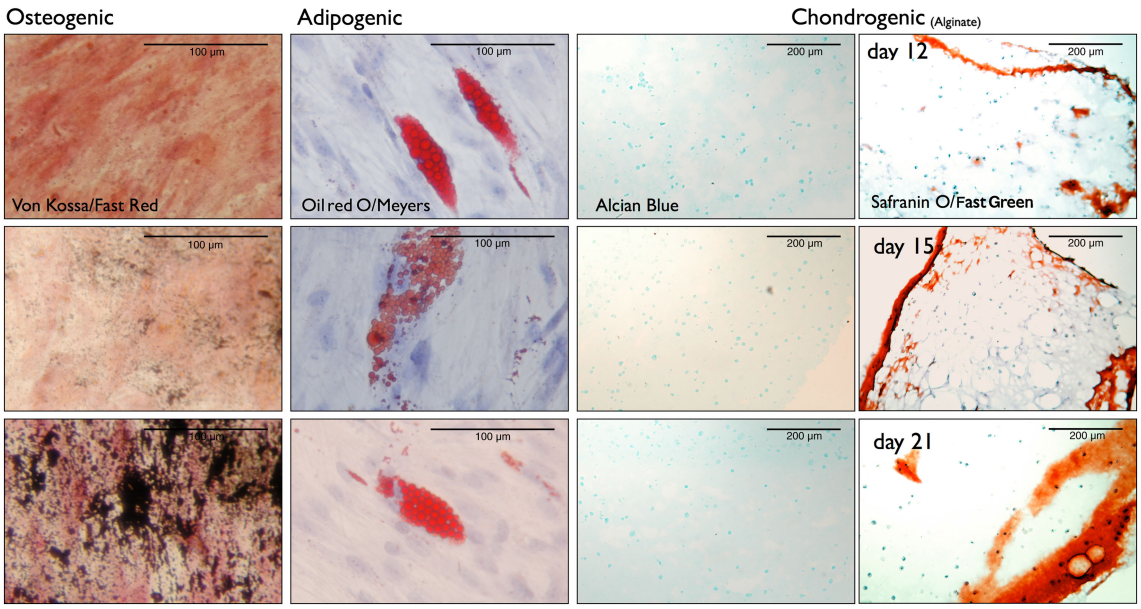

Figure 4. Histological stainings for each of the four differentiation lines of primary hMSCs after 12, 15 and 21 days. Column 1: osteogenic differentiation, von Kossa/fast red stain; column 2, adipogenic differentiation, oil red O/Meyer's haematoxylin; columns 3 and 4, chondrogenic differentiation, alcian blue and safranin O/fast green

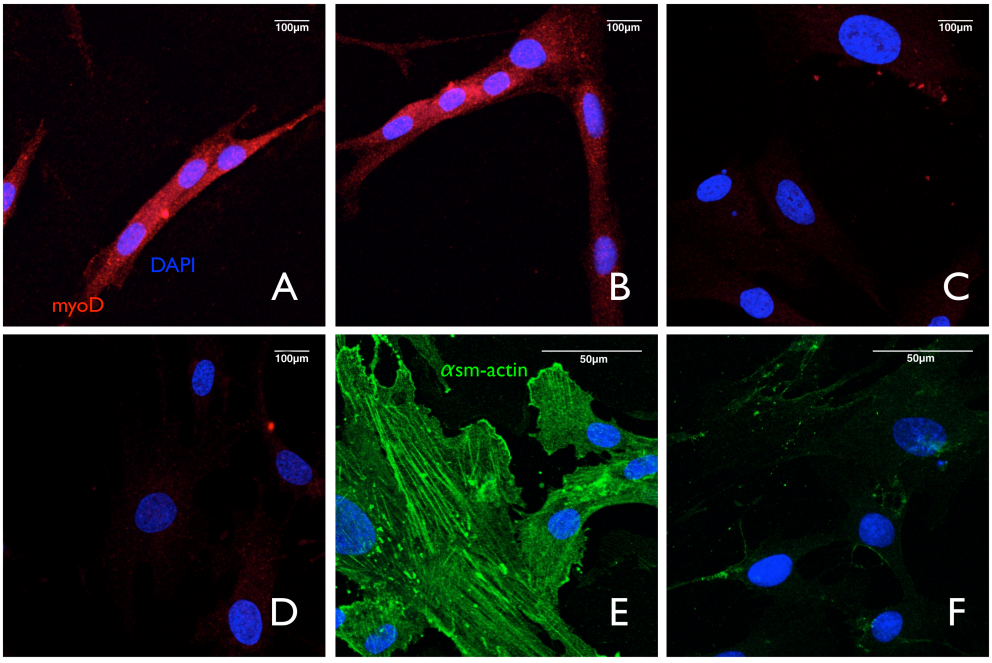

Figure 5. Confocal laser scanning microscope images of MyoD stain (Alexa555) and for α-smooth muscle actin stain (FITC) for myogenic differentiation and negative controls; nuclei were counterstained with DAPI. (A, B) Myotube formation after 14 days of culture, expressing MyoD; (C) negative control; (D) positive stain for undifferentiated control; (E) positive staining for α-smooth muscle (sm) actin of myogenic differentiation; (F) negative control

identified to be the main classifier for myogenic differentiation as well as 'fingers', i.e. filopodia (Figure 6D). Fingers were important to distinguish myogenic from all other cell differentiations, i.e. control, adipogenic and osteogenic. No clusters were identified for the other three differentiation groups compared to all others (data not shown).

4. Discussion

4.1. Differentiation of stem cells and correlation with cell shape

It seems evident that expansion of primary cells is a crucial step for the application of stem cell therapy

Copyright © 2012 John Wiley & Sons, Ltd.

DOI: 10.1002/term

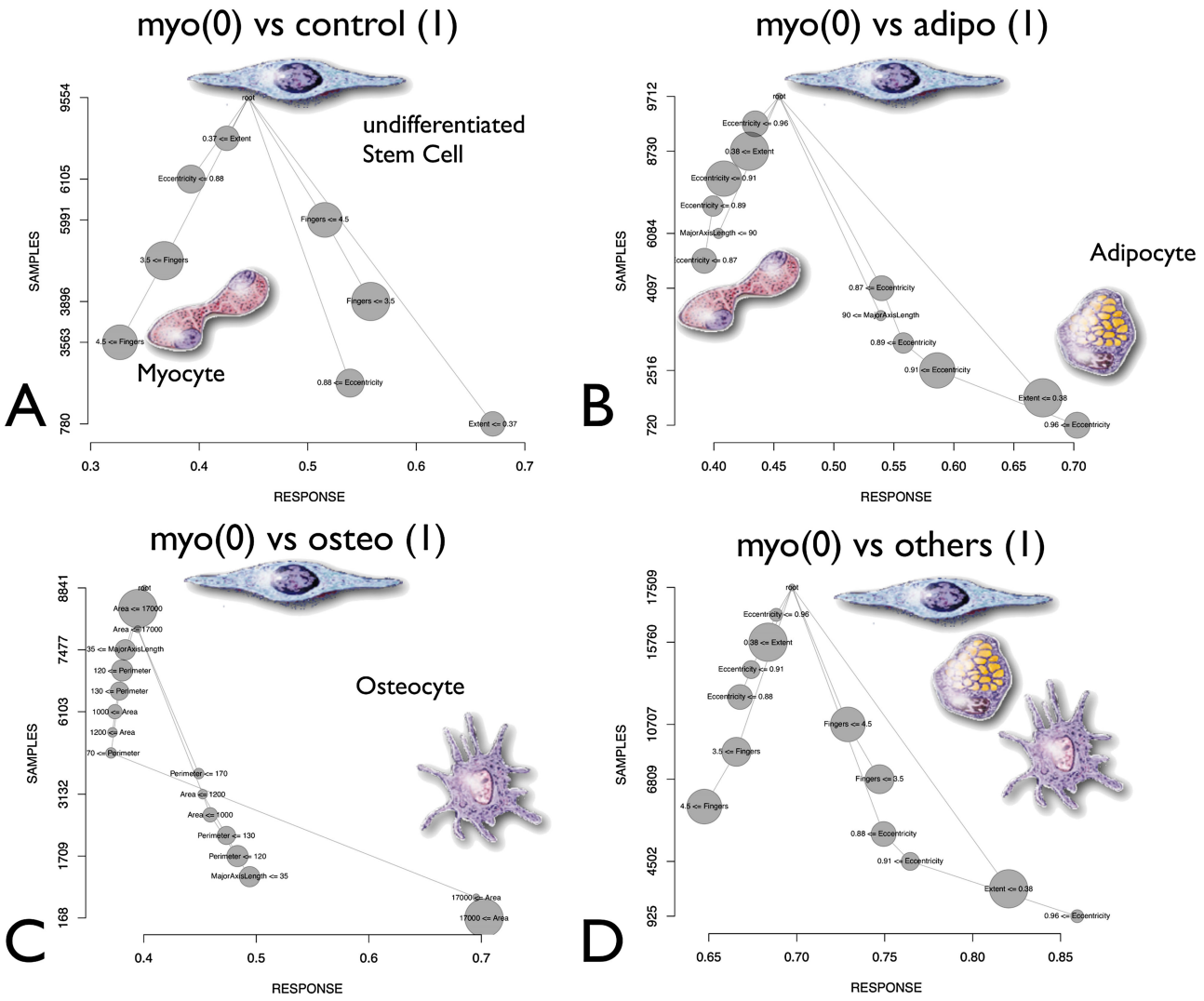

Figure 6. Output of node harvest classification method. The response axis represents: (A) myogenic = 0 and control = 1; (B) myogenic = 0 and adipogenic = 1; (C) myogenic = 0 and osteogenic = 1; (D) myogenic = 0 and adipogenic/osteogenic/control = 1; where values between 0 and 1 represent a weighted combination of both types. The sample axis indicates the number of cells. Each node contains cells that fulfil one condition of one element of the seven-feature vector; the node size shows the relevance of that condition and lines between nodes symbolize subsets

(Majd *et al*., 2008; Sarugaser *et al*., 2009; da Silva Meirelles *et al*., 2008). Here we demonstrate that modern time-lapse microscopy could be a potential tool to predict stem cell fate (Lutolf *et al*., 2009). We could successfully sort out the myogenic differentiation pattern from the, adipogenic, osteogenic and undifferentiated control cells, based solely on morphological feature vector. We could demonstrate that with the onset of myogenic differentiation (during the first 48 h of cell expansion), primary hMSCs undergo changes in eccentricity and cells undergoing myogenic fusion have an increased number of 'filopodia'. The two features 'eccentricity' and 'finger' (= filopodia) were significantly higher in early myogenic differentiation than in all other groups, as picked up by the Meinshausen (2010) classification algorithm. Of course, cell shape can change for many reasons; change in pH, limited nutrition, changes in osmolality, cell density and possibly others. However, over a large set of cells and in a controlled environment, such as laboratory standard plastics, it should be feasible to predict an average cell type using the proposed statistical stem cell methodology. Furthermore, it is known that primary hMSCs are always a heterogeneous cell population. Although our cells possessed the typical CD markers on their cell surfaces, as expected for stromal cells at the third passage, it is of course obvious that various phenotypes of stem cells might still be present in the populations and causing high variance of cell shapes. Also the ratio between differentiated and undifferentiated cells might run at different speeds among the four differentiation groups. The application of reporter systems is a very useful tool to visualize the reorganization of the cells. However, transfection of cells with a cytomegalovirus (CMV) promoter-based expression system might of course influence the behaviour and thus the shape of primary cells (Raimondo *et al*., 2006). Here, the development of a negative reporter system for *nanog* could be very helpful tool to distinguish undifferentiated cell from those undergoing differentiation (Pierantozzi *et al*., 2010).

Copyright © 2012 John Wiley & Sons, Ltd.

DOI: 10.1002/term

4.2. Cell classification pipeline

There are three parts to the classification pipeline: segmentation, feature selection and classification. The performance of each part depends on the performance of the previous one.

In the segmentation step, we did not consider the time of acquisition associated with each image. By tracking cells over time we could potentially improve the robustness of our cell segmentation algorithm (Gilbert *et al*., 2010). However, we noticed that taking a picture every 2 h is not enough to trace individual hMSCs over time, as has been recently proposed (Gilbert *et al*., 2010). This was not possible with the chosen time-lapse microscope set-up. Cell density certainly affected cell shape, a factor that was considered by our segmentation routine by excluding cells, which were connected to the edges of the images.

In the feature selection step, we could consider more morphological parameters or even intensity patterns. Furthermore, we believe that stem cell fate prediction can be enhanced by taking into account different scales of modelling, considering not only local characteristics of cell shape but also their interaction with and within a group of neighbouring cells (i.e. from individual to group modelling).

In the classification step, we chose a robust technique that is easy to interpret, which, given the nature of our data, is a reasonable choice. To get a relative performance measure it would be interesting to compare it to other methods, such as tree-clustering methods (Morris *et al*., 2011).

4.3. Cell shape predictors

Other approaches to characterize change in cell shape were followed in other studies. For instance, Glauche *et al*. (2009) attempted to quantify changes in tree topologies using mother–daughter cell phylogenies or (Cohen *et al*., 2010; Ravin *et al*., 2008) by application of a relatively well-defined differentiation process of neuronal precursor cells. Klauschen *et al*. (2009) recently attempted to reconstruct cell surface modifications to predict cell shape in three dimensions. Two-dimensional (2D) cell tracking seems a relatively easy approach to undertake (Gilbert *et al*., 2010). Our study is limited in the sense that we did not extensively clone bone-marrow cells by limiting dilution to exclude further variance of cell shape caused by a cell population mixture (Mareddy *et al*., 2007). In contrast, our primary aim was to test the feasibility of predicting differentiation solely by means of non-invasive image processing of cell shape. The limitation is the high cell density culture as it is obtained for confluence $> 70\%$. Future experiments should involve cell cycle synchronization during differentiation by hydroxyurea or colchicine in order to sort out cell shape changes from cell division (Lee *et al*., 2011; Banfalvi, 2011). Another approach to predicting stem cell fate non-invasively might be to use membrane polarity. Recently, it has been noticed that undifferentiated and differentiated cells differ in their polarity (Sundelacruz *et al*., 2009; Flanagan *et al*., 2008; Levin, 2007). Undifferentiated cells have different 'fate potentials' than differentiated cells (Flanagan *et al*., 2008). It remains to be shown whether hMSCs can be discriminated by different dielectric properties and whether the change in potential is a unique feature of each of the mesenchymal differentiation pathways (Sundelacruz *et al*., 2008). Possibly a combination of image-processing techniques together with recording of membrane potential could be the most promising step towards non-invasive prediction of stem cell fate.

5. Conclusions

In this study we demonstrated the potential to distinguish hMSCs differentiation from others through a classification of 7D feature vectors extracted from cells obtained from non-invasive time-lapse microscopy. In particular, the proposed segmentation pipeline and the node harvest classification algorithm picked up myogenic from all other cell differentiation pathways, which is prominent in pairwise comparisons (Figure 6). It remains to be shown whether this classification approach works out for large datasets, including donor variation and different cell sources (i.e. adipose, bone marrow). Other features have not been successfully identified to discriminate osteo-progenitor cells from adipose cells. With new time-lapse technologies emerging and more high-throughput data collection, new options to follow cells are possible. In addition, tracking cells in 3D opens new future challenges and possibilities.

Acknowledgements

Ladina Ettinger and Elena Calandriello assisted in histological staining. Rainer Egli provided protocols for CD marker characterization of hMSCs.

References

Banfalvi G. 2011; Overview of cell synchronization. *Methods Mol Biol* **761**: 1–23.

Caplan AI. 1991; Mesenchymal stem cells. *J Orthop Res* **9**(5): 641–650.

Caplan AI. 2005; Review: mesenchymal stem cells: cell-based reconstructive therapy in orthopedics. *Tissue Eng* **11**(7–8): 1198–1211.

Chamberlain JS. 2006; Stem-cell biology: a move in the right direction. *Nature* **444** (7119): 552–553.

Cohen AR, Gomes FL, Roysam B *et al*. 2010; Computational prediction of neural progenitor cell fates. *Nat Methods* **7**(3): 213–218.

Dainiak MB, Kumar A, Galaev IY *et al*. 2007; Methods in cell separations. *Adv Biochem Eng Biotechnol* **106**: 1–18.

da Silva Meirelles L, Caplan AI, Nardi NB. 2008; In search of the *in vivo* identity of mesenchymal stem cells. *Stem Cells* **26** (9): 2287–2299.

Copyright © 2012 John Wiley & Sons, Ltd.

Dominici M, Blanc KL, Mueller I *et al*. 2006; Minimal criteria for defining multipotent mesenchymal stromal cells. The International Society for Cellular Therapy position statement. *Cytotherapy* **8**(4): 315–315.

Flanagan LA, Lu J, Wang L *et al*. 2008; Unique dielectric properties distinguish stem cells and their differentiated progeny. *Stem Cells* **26**(3): 656–665.

Gantenbein-Ritter B, Benneker LM, Alini M *et al*. 2011; Differential response of human bone marrow stromal cells to either TGFβ(1) or rhGDF-5. *Eur Spine J* **20**: 962–971.

Gilbert PM, Havenstrite KL, Magnusson KE *et al*. 2010; Substrate elasticity regulates skeletal muscle stem cell self-renewal in culture. *Science* **329**(5995): 1078–1081.

Giordano A, Galderisi U, Marino IR. 2007; From the laboratory bench to the patient's bedside: an update on clinical trials with mesenchymal stem cells. *J Cell Physiol* **211**(1): 27–35.

Glauche I, Lorenz R, Hasenclever D *et al*. 2009; A novel view on stem cell development: analysing the shape of cellular genealogies. *Cell Prolif* **42**(2): 248–263.

Gorelick L, Galun M, Sharon E *et al*. 2006; Shape representation and classification using the poisson equation. *IEEE Trans Pattern Anal Mach Intell* **28**(12): 1991–2005.

Klauschen F, Qi H, Egen JG *et al*. 2009; Computational reconstruction of cell and tissue surfaces for modeling and data analysis. *Nat Protoc* **4**(7): 1006–1012.

Lee, WC, Bhagat, AA, Huang, S *et al*. 2011; High-throughput cell cycle synchronization using inertial forces in spiral microchannels. *Lab Chip* **11**(7): 1359–1367.

Levin, M. 2007; Large-scale biophysics: ion flows and regeneration. *Trends Cell Biol* **17**(6): 261–270.

Livak, KJ, Schmittgen, TD. 2001; Analysis of relative gene expression data using real-time quantitative PCR and the $^{2\Delta\Delta}C_T$ method. *Methods* **25**(4): 402–408.

Lutolf MP, Gilbert PM, Blau HM. 2009; Designing materials to direct stem-cell fate. *Nature* **462**(7272): 433–441.

Majd H, Wipff PJ, Buscemi L *et al*. 2008; A novel method of dynamic culture surface expansion improves mesenchymal stem cell proliferation and phenotype. *Stem Cells* **27**(1): 200–209.

Mareddy S, Broadbent J, Crawford R *et al*. 2009; Proteomic profiling of distinct clonal populations of bone marrow mesenchymal stem cells. *J Cell Biochem* **106**(5): 776–786.

Mareddy S, Crawford R, Brooke G *et al*. 2007; Clonal isolation and characterization of bone marrow stromal cells from patients with osteoarthritis. *Tissue Eng* **13** (4): 819–829.

Mehlhorn AT, Schmal H, Kaiser S *et al*. 2006; Mesenchymal stem cells maintain TGF-β-mediated chondrogenic phenotype in alginate bead culture. *Tissue Eng* **12** (6): 1393–1403.

Meinshausen N. 2010; Node harvest. *Ann Appl Stat* **4**(4): 2049–2072.

Morris JH, Apeltsin L, Newman AM *et al*. 2011; clusterMaker: a multi-algorithm clustering plugin for Cytoscape. *BMC Bioinformat* **12**: 436.

Pierantozzi E, Gava B, Manini I *et al*. 2010; Pluripotency regulators in human mesenchymal stem cells: expression of NANOG but not of OCT-4 and SOX-2. *Stem Cells Dev* **20**(5): 915–923.

Pittenger MF. 2008; Mesenchymal stem cells from adult bone marrow. *Methods Mol Biol* **449**: 27–44.

Pittenger MF, Mackay AM, Beck SC *et al*. 1999; Multilineage potential of adult human mesenchymal stem cells. *Science* **284**(5411): 143.

Prockop DJ. 1997; Marrow stromal cells as stem cells for nonhematopoietic tissues. *Science* **276**(5309): 71–74.

Prockop DJ. 2001; Stem cell research has only just begun. *Science* **293**(5528): 211–212.

Raimondo S, Penna C, Pagliaro P *et al*. 2006; Morphological characterization of GFP stably transfected adult mesenchymal bone marrow stem cells. *J Anat* **208**(1): 3.

Ravin R, Hoeppner DJ, Munno DM *et al*. 2008; Potency and fate specification in CNS stem cell populations *in vitro*. *Cell Stem Cell* **3**(6): 670–680.

Roeder I, Radtke F. 2009; Stem cell biology meets systems biology. *Development* **136** (21): 3525–3530.

Sarugaser R, Hanoun L, Keating A *et al*. 2009; Human mesenchymal stem cells self-renew and differentiate according to a deterministic hierarchy. *PLoS One* **4**(8): e6498.

Schmittgen TD, Zakrajsek BA. 2000; Effect of experimental treatment on housekeeping gene expression: validation by real-time, quantitative RT–PCR. *J Biochem Biophys Methods* **46**(1–2): 69–81.

Sengers BG, Dawson JI, Oreffo RO. 2009; Characterization of human bone marrow stromal cell heterogeneity for skeletal regeneration strategies, using a two-stage colony assay and computational modeling. *Bone* **46**(2): 496–503.

Solchaga LA, Johnstone B, Yoo JU *et al*. 1999; High variability in rabbit bone marrow-derived mesenchymal cell preparations. *Cell Transpl* **8**(5): 511–519.

Sundelacruz S, Levin M, Kaplan DL. 2008; Membrane potential controls adipogenic and osteogenic differentiation of mesenchymal stem cells. *PLoS One* **3**(11): e3737.

Sundelacruz S, Levin M, Kaplan DL. 2009; Role of membrane potential in the regulation of cell proliferation and differentiation. *Stem Cell Rev Rep* **5**(3): 231–246.

Zuk PA, Zhu M, Mizuno H *et al*. 2001; Multilineage cells from human adipose tissue: implications for cell-based therapies. *Tissue Eng* **7**(2): 211–228.

Copyright © 2012 John Wiley & Sons, Ltd.

DOI: 10.1002/term